ELSEVIER

Fluid Phase Equilibria 194–197 (2002) 309–317

FLUID PHASE EQUILIBRIA

www.elsevier.com/locate/fluid

Non-equilibrium molecular dynamics simulation study of the behavior of hydrocarbon-isomers in silicalite

S. Furukawa [a,b,*], C. McCabe [a,c], T. Nitta [b], P.T. Cummings [a,c]

[a] *Department of Chemical Engineering, University of Tennessee, Knoxville, TN 37996-2200, USA*
[b] *Department of Chemical Science and Engineering, Graduate School of Engineering Science, Osaka University, Toyonaka, Osaka, 560-8531, Japan*
[c] *Chemical Technology Division, Oak Ridge National Laboratory, Oak Ridge, TN 37831, USA*

Received 15 March 2001; accepted 20 August 2002

Abstract

Molecular dynamics simulations have been carried out in order to investigate the adsorption and permeation phenomena of butane isomers through ZSM-5 membranes. Using the μVT ensemble configurational-bias Monte Carlo technique, we are able to determine the preferred locations of the butane isomers in the ZSM-5 channels. In permeation simulations, using the μVT ensemble non-equilibrium molecular dynamics method, the permeate fluxes of the butane isomers are obtained. We find that the permeabilities of the *n*-butane calculated from the permeate fluxes increase with increasing temperature. The density of *n*-butane in the ZSM-5 decreases in the permeation direction with a similar pressure–density relationship to that measured by the equilibrium adsorption isotherm of the *n*-butane.

Keywords: Configurational-bias Monte Carlo; Non-equilibrium molecular dynamics; Silicalite; Butane isomers; Inorganic membrane

1. Introduction

Understanding transport properties in porous media at the molecular level is important in chemical engineering fields, such as adsorption and membrane separation processes. Among these fields, inorganic membranes with pores at the nanoscale have captured much attention, since inorganic membranes, such as zeolite and silica gel, are known to have several advantages over their organic counterparts—specifically, stability to high temperature and pressure, stability to organic chemicals and high resistance to erosion [1–3].

Molecular simulation techniques, which consist of the Monte Carlo (MC) and molecular dynamics (MD) methods, have become powerful tools with which to study the static and dynamic properties of

* Corresponding author. Tel.: +1-865-974-0553; fax: +1-865-974-4910.
E-mail address: furukawa@cheng.es.osaka-u.ac.jp (S. Furukawa).

0378-3812/02/$ – see front matter
PII: S0378-3812(01)00670-7

molecular systems, respectively [4,5]. Non-equilibrium MD (NEMD) simulations permit the simulation of steady-state systems away from equilibrium and have been successfully used to predict and understand transport properties at the molecular level. In particular, the boundary-driven NEMD (BD-NEMD) method, which was first proposed by Hafskjold et al. [6], has been developed to simulate transport phenomena under gradients of temperature, chemical potential or density. Two versions of the BD-NEMD method, the dual control volume grand canonical MD (DCV-GCMD) method [7] and the μVT ensemble NEMD (μVT-NEMD) method [8], have been successfully applied to investigate permeation phenomena and separation mechanisms of inorganic membranes.

In previous work [8–12], simulations of the gas permeation through nanoporous carbon membranes were carried out by using the μVT-NEMD method. Our latest results [12] suggested that the selectivity for permeation depends on the differences in permeation resistance and relative adsorption power for each component: high selective adsorption followed by selective diffusion rate through the membrane.

In this paper, we attempt to investigate the permeation phenomena of butane isomers in a ZSM-5 silicalite membrane through molecular simulation. Hydrocarbon isomers have almost the same thermodynamic properties, though the minimum molecular diameter of branched hydrocarbons is slightly larger than that of normal hydrocarbons. Hence, using molecular sieve membranes such as silicalite, which have a controlled pore size, is one way to separate mixtures composed of hydrocarbon isomers. However, the permeation mechanism for hydrocarbons in silicalite membranes is not clear.

2. Model

The transferable potentials for phase equilibria (TraPPE) model [14,15] is used to model the butane isomers. In the TraPPE model, the geometry of a butane molecule is described by using a united-atom model where each CH_3 and CH_2 group is considered as a single spherical interaction site in the model. Inter-molecular interactions between the sites of butane molecules are calculated by the 12-6 Lennard–Jones (LJ) potential,

$$u_{\mathrm{LJ}}(r_{ij}) = 4\varepsilon_{ij}\left[\left(\frac{\sigma_{ij}}{r_{ij}}\right)^{12} - \left(\frac{\sigma_{ij}}{r_{ij}}\right)^{6}\right] \tag{1}$$

where r_{ij}, σ_{ij} and ε_{ij} are the distance, the size and energy parameters of the 12-6 LJ potential, for the pair of sites i and j, respectively. The cross parameters are calculated from the Lorentz–Bertherot combining rule. For intramolecular interactions, motions of the bond bending angles (θ) and the dihedral angles (ϕ) in the butane molecule are governed by the harmonic and torsional potentials as follows:

$$u_{\mathrm{bend}}(\theta) = \frac{k_\theta(\theta - \theta_0)^2}{2} \tag{2}$$

where k_θ, and θ_0 are the bond bending force constant and equilibrium bond angle, respectively, and

$$u_{\mathrm{torsion}}(\phi) = c_0 + c_1[1 + \cos\phi] + c_2[1 + \cos(2\phi)] + c_3[1 + \cos(3\phi)] \tag{3}$$

with $c_0 = 0$, $c_1 = 335.03$ J/mol, $c_2 = -68.19$ J/mol and $c_3 = 791.32$ J/mol. In our simulations, a bond stretching motion is also taken into consideration, using a simple harmonic potential.

$$u_{\mathrm{stretch}}(r_{ij}) = \frac{k_r(r_{ij} - r_0)^2}{2} \tag{4}$$

Table 1
Potential parameters used in this work (from [14,15,17])

Site	Mass (kg/mol)	σ (nm)	ε (J/mol)
CH_3	15.04×10^{-3}	0.375	814.8
CH_2	14.03×10^{-3}	0.395	382.4
CH_3–O (ZSM-5)	–	0.360	665.1
CH_2–O (ZSM-5)	–	0.360	482.2
Bond bending	θ_0 (°)	k_θ (J/mol)	
CH_x–CH_2–CH_x	114	519625	
CH_x–CH–CH_x	112	519625	

where k_r is the bond stretching force constant ($=3.766 \times 10^{26}$ J/mol) and r_0 is the equilibrium bond length ($=0.154$ nm) [16].

The ZSM-5 zeolite is known from experimental studies to have straight and zigzag channels with channel intersections [13]. Pore sizes for the straight channel (0.54 nm × 0.56 nm) and the zigzag channel (0.51 nm × 0.54 nm) are almost the same as the smallest diameter of the butane isomers: 0.54 nm for the *n*-butane molecule and 0.63 nm for the *iso*-butane molecule under the optimized geometry. The structure of the model ZSM-5 in our simulations is a rigid crystal based on experimental geometry data. For interactions between butane molecules and the ZSM-5, only pairs of sites in butane molecules and oxygen atoms in the ZSM-5 are considered.

The potential model parameters used to model both the butane isomers and ZSM-5 membrane are summarized in Table 1.

3. Simulation methods

3.1. μVT-CBMC method

The μVT-MC simulation technique is a popular method with which to investigate adsorption equilibrium in porous materials. However, with the conventional μVT-MC technique it is difficult to obtain reasonable fractions of acceptances for molecular displacements or insertions at high adsorption densities, especially for complex fluids. As a technique to solve these problems, in particular, to perform simulations of chain molecules in porous materials, the μVT-CBMC technique [5] has been developed. In this technique, instead of the random displacement or insertion of a molecule, a molecule is grown atom by atom while interacting with other molecules in the system. As the molecule is grown, the acceptance probability of the molecular geometry and that of the conformation are calculated from the intra- and inter-molecular potential energies, respectively. In brief, the μVT-CBMC method involves four moves as follows.

1. random displacement of a molecule based on the center of mass;
2. random rotation of a molecule around the center of mass;
3. re-growth of a part of the molecule selected randomly;
4. insertion or deletion of a molecule; the conformation for an inserted molecule and the choice of a deleted molecule are selected randomly.

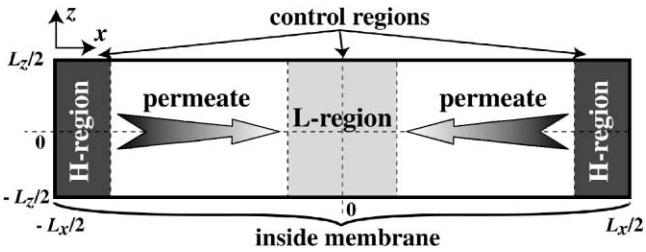

Fig. 1. A schematic diagram of a simulation cell for the μVT-NEMD method.

During the simulations, the distribution of these four operations attempted in a MC block, is 30% displacements, 30% rotations, 10% chain re-growths and 30% insertions or deletions. All the simulations were run for 4000 MC blocks, with 1000 cycles per MC block. The ensemble averages of the macroscopic properties were calculated from the simulation results for the last 1000 MC blocks.

3.2. μVT-NEMD method

Fig. 1 shows a schematic diagram of a simulation cell for the μVT-NEMD method. The cell consists of two mirror-image symmetric boxes in order to satisfy the periodic boundary condition in the permeating (*x*-) direction. Each symmetric box has three regions: the H-region (high density) and L-region (low density) which are both density-controlling, and the M-region located between the H-region and the L-region which is free of control. The ZSM-5 membrane exists throughout the whole simulation cell.

During a simulation run, the densities in the H- and L-regions are kept constant at specified values using the insertion and deletion algorithms of the μVT-CBMC method. The specified densities, which are in equilibrium with bulk gases at specified pressures, P_H and P_L, are pre-determined by the μVT-CBMC method. The velocities of the inserted molecules are assigned values around the average velocity corresponding to the specified temperature by using random numbers on the Gaussian distribution. The insertion and deletion operations are carried out each 20 MD steps. Molecular translation velocities are rescaled independently after insertion and deletion operations in order to maintain a constant temperature. Molecules move from the H-region to the L-region through a multiple time step molecular dynamics algorithm [18], and a non-equilibrium stationary state is obtained in the M-region. The MD time steps we adopted are 1.0 fs for the large time step and 0.4 fs for the small time step. To calculate ensemble averages, simulation results for the last 3,000,000 time steps of a 5,000,000 time step run are used.

4. Results and discussion

4.1. Adsorption phenomena of butane isomers in ZSM-5

Fig. 2 shows adsorption isotherms for pure *n*- and *iso*-butanes in the ZSM-5 at 300 K compared with experimental data [19]. From the figure we see that the adsorption density for the butane isomers increase with increasing pressure, exhibiting Langmuir-type behavior. At each pressure, the density of *n*-butane is always larger than that of *iso*-butane, which we attribute to the difference in the molecular geometry of the two molecules. The simulation results are in excellent agreement with the experimental data for

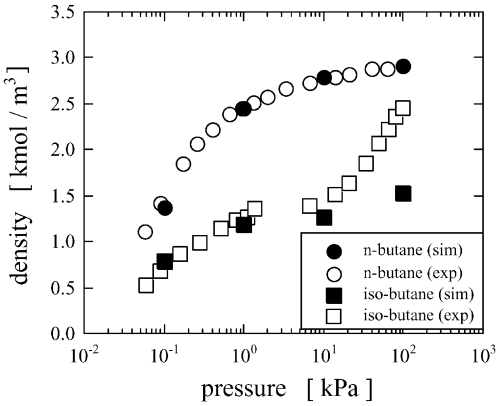

Fig. 2. Adsorption isotherms for pure *n*-butane (circles) and *iso*-butane (squares) at 300 K.

n-butane at all pressures and at low pressures for isobutane. The simulation results for isobutane over predicts the adsorption density at higher pressures.

In order to gain more insight into the local density in the ZSM-5 pores, the probability distributions of each butane isomer in the straight and zigzag channels and their intersection are calculated from the results of μVT-CBMC simulations (Fig. 3). In the case of *n*-butane, we find there is a greater probability of finding the molecules in the straight and zigzag channels compared to the intersections. In addition, the probabilities in the straight and zigzag channels are almost the same. However, in the case of *iso*-butane, most molecules are located at intersections, with only a small fraction being found in the zigzag and straight channels. The probability of finding an *iso*-butane molecule in the straight channel is considerably smaller than that in the zigzag channel. With increasing pressure, the probability of finding an *iso*-butane

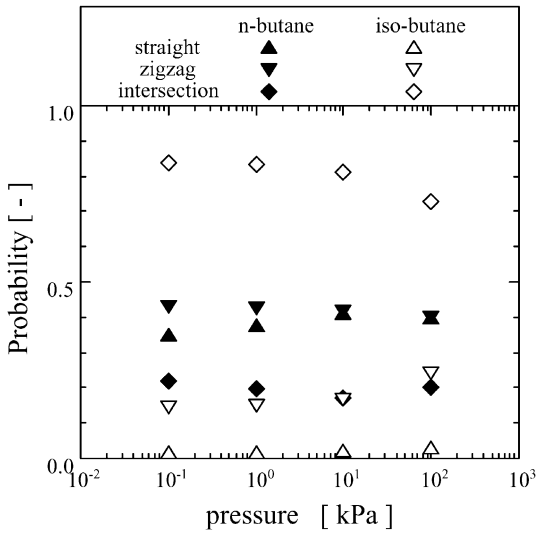

Fig. 3. Probability distributions of *n*-butane (closed symbols) and *iso*-butane (open symbols) at 300 K.

Table 2
Equilibrium densities (kmol/m^3) in the H- and L-regions

	300 K		400 K	
	1.0 kPa (ρ_L)	100 kPa (ρ_H)	1.0 kPa (ρ_L)	100 kPa (ρ_H)
n-Butane	2.57	2.91	0.10	2.07
iso-butane	1.21	1.66	0.10	1.12

molecule in the intersection decreases, while that in the zigzag channel increases. These findings for the packing of the butane isomers in the ZSM-5 are in agreement with the suggestions of [20,21] based on experimental analysis.

4.2. Permeation phenomena of butane isomers in ZSM-5

Permeation simulations of pure butane isomers through the ZSM-5 are carried out at the following conditions: 300 and 400 K, $P_H = 100$ kPa and $P_L = 1.0$ kPa, and membrane thickness $L_m = 5.976$ nm. The (0 1 0) surface is set as a permeation surface, namely there are straight channels toward the permeation direction and zigzag channels perpendicular to the permeation direction. Equilibrium densities calculated by the μVT-CBMC simulations are used to determine the densities in the H- and L-regions (Table 2).

Fig. 4 shows a snapshot of pure *n*-butane in ZSM-5 at 400 K. The snapshot is a view of the (0 0 1) surface, and the permeation direction is from left to right. We see that the *n*-butane molecules locate in both the straight (*x*-direction) and zigzag channels (*z*-direction). Fig. 5 shows density profiles for the *n*-butane at 300 and 400 K. In both figures, there are two peaks; the high peaks correspond to the locations of zigzag channels and intersections and the much lower peaks to the straight channels. The higher and lower peaks decrease toward the permeation direction, particularly at the higher temperature studied. In the case at 400 K, the higher peaks decrease rapidly toward the permeation direction showing a similar pressure–density relationship to that measured by the equilibrium adsorption isotherm.

The membrane permeabilities ($\hat{P}$) are calculated from permeate fluxes using the relation

$$\hat{P} = \frac{JL_m}{\Delta P} \tag{5}$$

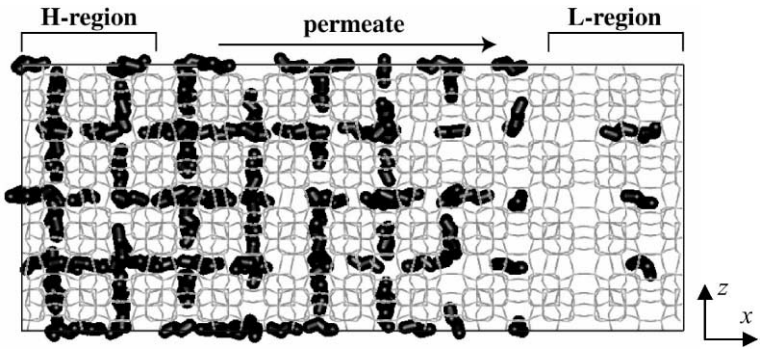

Fig. 4. Snapshot of pure *n*-butane in ZSM-5 at 400 K.

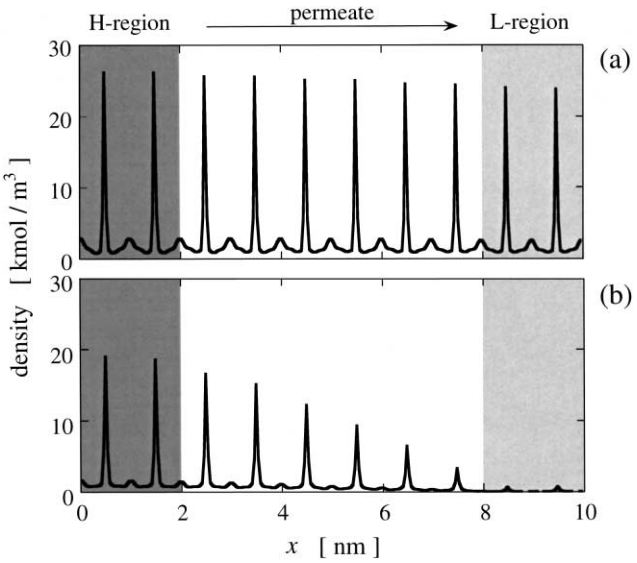

Fig. 5. Density profiles of pure *n*-butane permeation at (a) 300 and (b) 400 K.

Table 3
Permeabilities from simulation and experiment [20] for *n*-butane

Temperature (K)	Permeability (mol m/m^2 Pa)	
	Simulation	Experiment
300	3.44×10^{-10}	2.50×10^{-12}
400	3.95×10^{-10}	5.00×10^{-12}

where J is the permeate flux, L_m is the membrane thickness and ΔP is the pressure difference across the membrane. The permeabilities are summarized in Table 3 along with experimental data [20]. The permeability of *n*-butane at 400 K is larger than that at 300 K. This is because, as the temperature goes from 300 to 400 K, the increase in the mobility is larger than the decrease in the adsorption power. Compared to the experimental data, the permeabilities obtained from the simulations are much larger. However, it is encouraging to observe that the increase in the permeability with increasing temperature is in agreement with the experimental trend.

In the cases of the *iso*-butane permeation at $T = 300$ and 400 K, simulation results at stationary states could not be obtained. Takaba et al. [22] also reported similar results by MD simulations.

5. Conclusion

A series of μVT-CBMC and μVT-NEMD simulations were carried out in order to investigate permeation phenomena of butane isomers through ZSM-5 membranes. From the results of the μVT-CBMC simulations, it has been found that the *n*-butane molecules prefer to locate in the straight and zigzag chan-

nels of the ZSM-5 with almost the same probabilities, while most of the *iso*-butane molecules locate at the intersection of the channels. In permeate simulations of the *n*-butane using the μVT-NEMD method, the densities in the ZSM-5 decreased exhibiting a similar pressure–density relationship to that measured by the equilibrium adsorption isotherm. In the case of the *iso*-butane permeation, density profiles and permeate fluxes at stationary states for the *iso*-butane were not obtained. For studying transport properties of the *iso*-butane, it may be necessary to adopt a more detailed potential model for the atoms of the ZSM-5 which includes motion of the atoms in the membrane.

List of symbols

c_i	parameter of torsion potential
k_r, k_θ	parameters of bond stretching and bending
L_m	membrane thickness
$\hat{P}$	permeability
P_H, P_L	pressures at H- and L-regions
r	distance
T	temperature
u	potential energy

Greek letters

ε, σ	LJ size and energy parameters
ϕ	dihedral angle
θ, θ_0	bond angle and equilibrium bond angle
ρ_H, ρ_L	densities at H- and L-regions

Acknowledgements

The research was partly supported by the Research Fellowships of the Japan Society for Promotion of Science for Young Scientists, Japan.

References

[1] R.R. Bhave (Ed.), Inorganic Membranes, Synthesis, Characterization, and Application, Van Nostrand Reinhold, New York, USA, 1991.
[2] H.P. Hsieh, Inorganic Membranes for Separation and Reaction, Elsevier, Amsterdam, 1996.
[3] A.J. Burggraaf, L. Cot (Eds.), Fundamentals of Inorganic Membrane Science and Technology, Elsevier, Amsterdam, 1996.
[4] M.P. Allen, D.J. Tildesley, Computer Simulation of Liquids, Clarendon Press, Oxford, 1987.
[5] D. Frenkel, B. Smit, Understanding Molecular Simulation, From Algorithm to Applications, Academic Press, San Diego, 1996.
[6] B. Hafskjold, T. Ikeshoji, S.K. Ratkje, Mol. Phys. 80 (1993) 1389–1412.
[7] G.S. Heffelfinger, F. van Swol, J. Chem. Phys. 101 (1994) 7548–7552.
[8] S. Furukawa, T. Shigeta, T. Nitta, J. Chem. Eng. Jpn. 29 (1996) 725–728.
[9] S. Furukawa, T. Nitta, J. Chem. Eng. Jpn. 30 (1997) 116–122.
[10] S. Furukawa, K. Hayashi, T. Nitta, J. Chem. Eng. Jpn. 30 (1997) 1107–1112.
[11] S. Furukawa, T. Sugahara, T. Nitta, J. Chem. Eng. Jpn. 32 (1999) 223–228.
[12] S. Furukawa, T. Nitta, J. Membr. Sci. 178 (2000) 107–119.

[13] C.R.A. Catlow, Modeling of Structure and Reactivity in Zeolites, Academic Press, London, 1992.
[14] M.G. Martin, J.I. Siepmann, J. Phys. Chem. B 102 (1998) 2569–2577.
[15] M.G. Martin, J.I. Siepmann, J. Phys. Chem. B 103 (1999) 4508–4517.
[16] C.J. Mundy, J.I. Siepmann, M.L. Klein, J. Chem. Phys. 102 (1995) 3376.
[17] T.J.H. Vlugt, R. Krishna, B. Smit, J. Phys. Chem. B 103 (1999) 1102–1118.
[18] M.E. Tuckerman, B.J. Berne, G.J. Martyna, J. Chem. Phys. 102 (1992) 1990–2001.
[19] M.S. Sun, O. Talu, D.B. Shah, J. Phys. Chem. 100 (1996) 17276–17280.
[20] W. Zhu, J.M. van de Graaf, L.J.P. van den Broeke, F. Kapteijn, J.A. Moulijn, Ind. Eng. Chem. Res. 37 (1998) 1934–1942.
[21] R.E. Richards, L.V.C. Rees, Langmuir 3 (1987) 335–340.
[22] H. Takaba, R. Koshita, K. Mizukami, Y. Oumi, N. Ito, M. Kubo, A. Fahmi, A. Miyamoto, J. Membr. Sci. 134 (1997) 127–139.